Exciton Structure and Energy Transfer in the Fenna-Matthews-Olson Complex

Thyrhaug, Erling; Zidek, Karel; Dostál, Jakub; Bína, David; Zigmantas, Donatas

Published in:
The Journal of Physical Chemistry Letters

DOI:
10.1021/acs.jpclett.6b00534

2016

Document Version:
Peer reviewed version (aka post-print)

Exciton Structure and Energy Transfer in the Fenna-Matthews-Olson Complex

Erling Thyrhaug[1], *Karel Žídek*[1], *Jakub Dostál*[1,2], *David Bína*[3], *Donatas Zigmantas*[1]*.

[1] - Department of Chemical Physics, Lund University, P.O. Box 124, 22100 Lund, Sweden

[2] – Institut für Physikalische und Theoretische Chemie, Universität Würzburg, Am Hubland, D-97074 Würzburg, Germany

[3] – Biology Centre CAS, Branišovská 31, and Faculty of Science, University of South Bohemia, Branišovská 1760, 370 05 České Budějovice, Czech Republic

Corresponding Author

* donatas.zigmantas@chemphys.lu.se

The Fenna-Matthews-Olson (FMO) photosynthetic complex found in green sulfur bacteria has over the last decades been one of the favorite "model" systems for biological energy transfer. Yet, even after 40 years of studies, quantitative knowledge about its energy transfer properties is limited. Here two-dimensional electronic spectroscopy (2DES) with full polarization control is used to provide an accurate description of the electronic structure and population dynamics in the complex. The sensitivity of the technique has further allowed us to spectroscopically identify the eight bacterio-chlorophyll molecule recently discovered in the crystal structure. The time evolution of the spectral structure, covering timescales from tens of femtoseconds up to a nanosecond, reflects the energy flow in FMO and enables us to extract an unambiguous energy transfer scheme.

TOC GRAPHICS

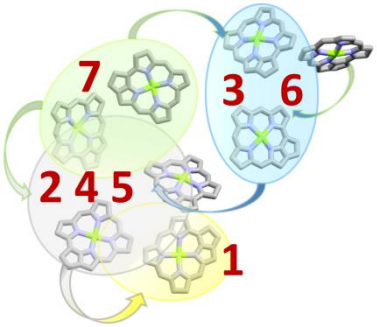

KEYWORDS Energy transfer, Photosynthesis, two-dimensional electronic spectroscopy, exciton diffusion

The Fenna-Matthews-Olson (FMO) complex is a small protein homo-trimer found in the photosynthetic apparatus of a number of green sulfur bacteria. It was among the first structurally well-characterized photosynthetic proteins, and has attracted attention from spectroscopists, theoreticians, and biologists for several decades. The scaffold of the protein supports bacteriochlorophyll a (BChl) pigments in a well-defined geometry, shaping its optical properties to appear substantially different from those of the constituent BChl molecules in solution. It is situated between the light-harvesting antenna chlorosome and the photosynthetic reaction center of the bacteria, and due to this positioning and its ladder-like energy-level structure it has been proposed to function as a "funnel" for harvested solar energy towards the reaction center.

Because of the compact and well known structure, FMO is a convenient and illuminating system to study for both experimentalists and theoreticians. It is water-soluble, its crystal structure has been known in increasing detail since 1975[1-2], and its relatively small size makes spectral analysis and theoretical modeling *in principle* tractable problems. These advantages have resulted in FMO becoming one of the most thoroughly studied light-harvesting complexes in photosynthetic research.[3] The incentive has been that by understanding the optical properties of this simple system one could achieve greater understanding of the mechanisms of photosynthetic energy transfer in general. However, even in this model system the situation has turned out to be more complicated than initially anticipated, and still, some 40 years after its isolation and characterization, considerable controversy persists about both its function and its fundamental photophysical properties. Exciton energies and their extent of delocalization are still debated, as is both the quantitative and qualitative aspects of energy transfer through the complex. More complex issues, such as the interpretation of quantum beats observed in its time

resolved spectroscopic signals[4-6] have both spurred considerable debate, and been among the important factors in initiating the field of quantum biology.

FMO variants from several different species of green sulfur bacteria have been studied in detail, and while some structural and spectroscopic differences are observed, all are C_3 symmetric protein trimers, each unit containing identical structures of 8 BChl pigments (see Figure 1A). One of these, BChl 8, is loosely bound to the protein surface and is typically lost during isolation and purification. As a result it was only recently discovered in the FMO crystal structure[2]. Some experimental efforts to identify its spectral contribution has been made[7], however the majority of work on the optical properties of this BChl have been theoretical[8-10], where more recent studies suggest that it contributes to the very blue edge of the absorption spectrum[8].

The *intra*-unit electronic coupling amongst BChl pigments in the protein is moderate (up to approximately 100 cm^{-1})[11-13]. The environment induced perturbations to the optical transitions are also substantial, which in sum results in a structured lowest energy absorption band, centered at ~810 nm and spanning some 40 nm, rather than the 780 nm band observed for BChl in solution[14]. *Inter*-unit coupling in the trimer on the other hand is relatively weak (below 20 cm^{-1} for all BChl pairs)[15-16], thus the short time optical response is that of the individual subunits rather than of the protein complex as a whole. As a result, the spectrum of FMO contains observable features originating from a system of 7 (or 8) excitons rather than of 21 (or 24) excitons one would expect with stronger *inter*-unit interaction. The energy spacing of the excitonic levels is relatively small (in the order of 5 nm) and the optical transitions show considerable inhomogeneous broadening, which results in severely congested spectra. The resulting linear absorption (LA) spectrum is almost entirely featureless at physiological

temperatures, but at cryogenic temperatures three distinct peaks emerge. In the FMO species investigated here, isolated from *Chlorobaculum tepidum*, these are found at 12120 cm^{-1} (825 nm), 12270 cm^{-1} (815 nm), and at 12420 cm^{-1} (805 nm), while an additional broad shoulder is found on the blue side at approximately 12650 cm^{-1} (790 nm).

The properties of FMO have been addressed with an array of optical techniques, ranging from steady-state absorption and fluorescence[3, 17] to spectral hole-burning[18-19] and a variety of pump-probe based techniques[20-22]. Nevertheless, the combination of closely-spaced energy levels and rapid energy transfer leaves FMO as a difficult sample to probe by conventional time-resolved techniques. The direct relationship between spectral bandwidth and pulse length implies that either spectral or temporal resolution must be sacrificed. It presents, however, a well suited system for two-dimensional electronic spectroscopy (2DES).

2DES was first implemented in the visible range in the end of the 90's[23-26], and has since proven to be a powerful time-resolved spectroscopy technique. The main strength of 2DES is its interferometric nature, relying on pumping by two interfering optical pulses followed by a single pulse – "probe". This three-pulse (plus a *local oscillator*) sequence enables the acquisition of a two-dimensional map with high spectral resolution in both "pump" and "probe" frequency axes for each population time without sacrificing high temporal resolution. Thus experiments are typically done using pulses of a few tens of femtoseconds or shorter. A particularly important demonstration of the capabilities of 2DES for studying complex systems was the visualization of electronic couplings in FMO isolated from *Chlorobaculum tepidum*.[27] This early study addressed the issue of correlations between states in the FMO electronic structure; however theoretical modeling[12] resulted in only qualitative agreement with experimental data, and no attempt at quantifying energy transfer rates or exciton correlations directly from experimental data were

made. Subsequent work has focused primarily on the coherent response of the system[5-6], thus an accurate experimental determination of electronic structure and population dynamics was lacking. Here we revisit the problem of electronic structure and relaxation dynamics in this protein complex with the help of polarization controlled high-resolution 2DES. We thus record 2D spectra using the magic-angle pulse sequence $\langle 54.7°, 54.7°, 0°, 0° \rangle$, where the sequence of four pulses of linear polarization angle Φ_i is denoted by $<\Phi_1,\Phi_2,\Phi_3,\Phi_4>$, over a broad range of population times (femtoseconds up to a nanosecond) covering the entire excited state lifetime window. Supplementary linear polarization schemes were used for detailed exciton structure determination, as described below. In total these extensive data sets allows for, by use of an in-house developed global-fitting routine, accurate analysis of the energy transfer processes in the excitonic state space.

We performed all experiments at cryogenic temperatures in the interest of obtaining a high degree of spectral resolution. Magic angle absorptive (real part of the signal) 2D spectra recorded at 77 K and at a range of representative population times are shown in Figure 1C. Representative 2D spectra at higher cryogenic temperatures can be found in the supporting information. The three main diagonal peaks in the short population time (100 fs) 2D spectrum are in good agreement both energetically and in shape with the corresponding features in LA and transient absorption spectra[28].

A number of positive off-diagonal features, so called cross-peaks, are observed in the 2D spectra. These correlate excitonic states on the diagonal, where above-diagonal features indicate shared ground state bleach (GSB), and below-diagonal features in addition contain stimulated emission (SE) signals, reporting on downwards energy transfer[23, 27].

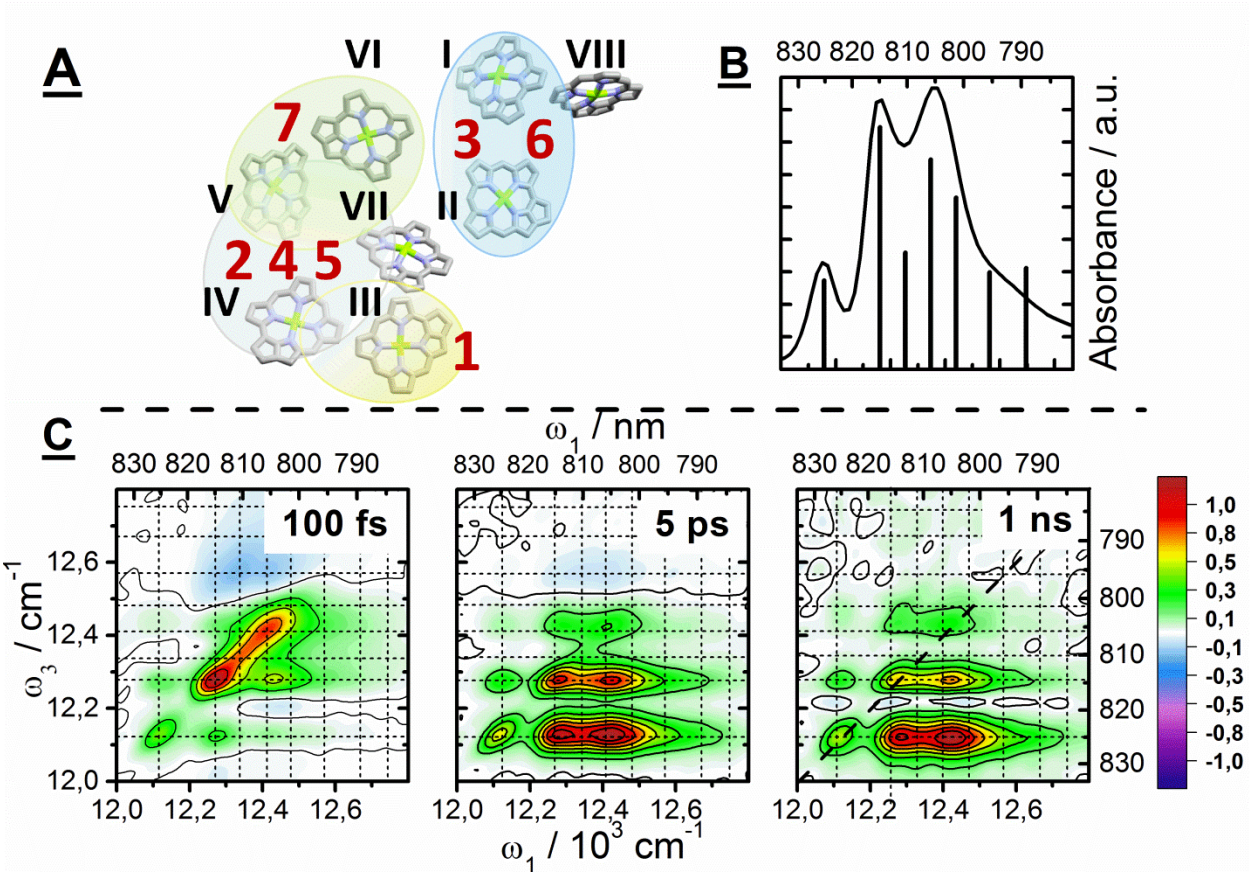

Figure 1: **A:** Arrangement of BChl a pigments within the FMO units. BChl site numbering according to Fenna in black Roman numerals. Schematic representation of spatial extent of the excitons according to Adolphs *et al.*[11] shown by shaded areas. Exciton numbering (red numbers) is given in order of increasing energy. **B:** linear absorption spectrum of FMO at 77 K with excitonic transitions (*vide infra*) represented by vertical bars. **C:** Normalized absorptive 2D spectra at increasing population delays with dashed lines indicating excitonic transition energies. All spectra were recorded in 1:2 aqueous buffer:glycerol mixture at 77 K.

In an extended excitonic system such as FMO, shared GSB in particular imply some spatial overlap of excitonic wavefunctions, which allows us to qualitatively discuss also the spatial extent of the excitons. In FMO all major diagonal features are connected by above-diagonal cross-peaks, indicating a large degree of spatial overlap of excitons, and thus significant

delocalization. Most simulations suggest delocalization over 2-3 BChl a sites for each exciton, *e.g.* the calculations by Adolphs and Renger[11] suggests spatial overlap between excitons **1**, **2**, **4**, and **5** at BChl a site IV (using Fenna's numbering). This situation is schematically illustrated in Figure 1, panel A, and is qualitatively consistent with our results. We note that exciton delocalization in FMO has been observed through shared GSB contributions also in transient absorption experiments.[21, 28]

While the 2D diagonal contains all optically active states in the system, the diagonal trace appears similar to the LA spectrum, thus assignment of the excitonic structure from this alone is impossible for FMO due to spectral congestion. The cross-peak spectral regions are often less congested, making 2DES very helpful in excitonic structure investigations since cross-peaks appear at coordinates directly corresponding to the energy of correlated exciton pairs. In many cases the energies (and correlations) of excitonic states can thus be simply read from the cross-peak coordinates. While this type of analysis is straightforward, in the case of FMO the considerable spectral congestion inhibits clear analysis even for such a procedure. A particularly large problem is the dominating diagonal signals, which hide or distort many of the relevant cross-peaks. A well-established approach to reducing congestion in linear and non-linear spectra is by exploiting polarization techniques[29-32]. We here modify Albrechts approach for separation of fluorescence excitation spectra into orthogonal components parallel and perpendicular to the emission[32-33]. The 2D analogue to this approach separates the spectrum into two components, polarized parallel and perpendicular to the "pumped" transition respectively. The 2D diagonal, being "pump" and "probe" interaction with identical pulses, and cross peaks between states of small relative projection angles are selectively amplified in the former ($\mathbf{S_Z}$) , while the latter ($\mathbf{S_Y}$) removes the diagonal entirely (and enhances cross-peaks at large projection angles), greatly

reducing the spectral congestion. We note that somewhat conceptually different approaches to generate spectra proportional to $\mathbf{S_Y}$ has been taken by Zanni and Hochstrasser[34] and Abramavicius and Mukamel[35]. Fleming and coworkers adapted the approach of Hochstrasser to 2DES[36], using the "cross-peak specific" pulse sequence $\boldsymbol{S_{CPS}} = \langle\frac{\pi}{3}, -\frac{\pi}{3}, 0,0\rangle$, which is directly proportional to $-\mathbf{S_Y}$. As there is no direct way to apply the projection theorem[23] to assign absolute phase to S_{CPS}, we prefer to use the expressions detailed below. Further comparisons and discussion of these approaches can be found in the supporting information. In the present approach we record the two polarized spectra $S_V = \langle 0,0,0,0\rangle$ and $S_H = \langle\frac{\pi}{2}, \frac{\pi}{2}, 0,0\rangle$. From these experimental spectra we generate "polarization associated spectra" (PAS) from the expressions[32-33]:

$$\boldsymbol{S_Z} = \frac{1}{3}(S_V + 2S_H)\left(5\frac{S_V - S_H}{S_V + 2S_H} + 1\right) = MA(5r_0 + 1)$$

$$\boldsymbol{S_Y} = \frac{1}{3}(S_V + 2S_H)\left(2 - 5\frac{S_V - S_H}{S_V + 2S_H}\right) = MA(2 - 5r_0)$$

Here MA is the spectrum recorded at the magic angle conditions, and r_0 is the 2D analogue to the fluorescence (or pump-probe) anisotropy. Representative PAS maps at two temporally well-separated times are shown in Figure 2. The decomposition of the total spectrum into two orthogonal components substantially reduces spectral congestion, and allows for the cross-peak positions to be determined unambiguously by the simple cross-peak "triangulation" approach outlined above (exciton energy identification is shown explicitly in SI Figure S2). The resulting excitonic energy levels are shown as gridlines in the spectra in Figure 2, where individual cross- (and diagonal-) peaks can be found at the grid vertices.

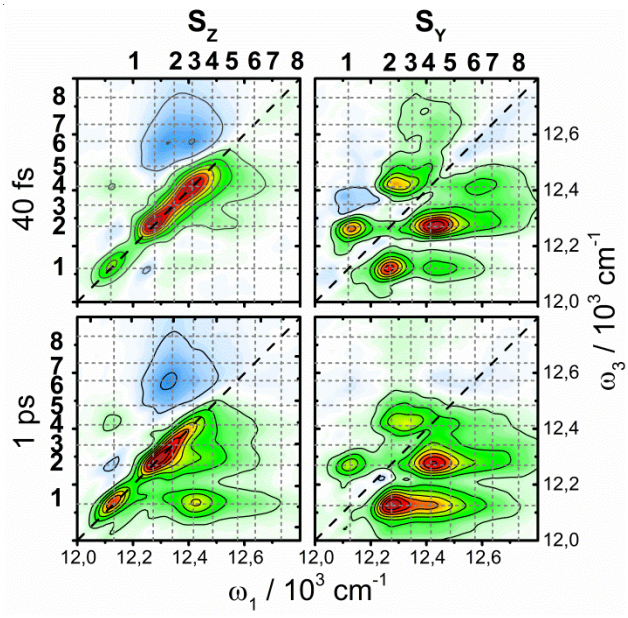

Figure 2: Normalized polarization associated spectra $\mathbf{S_Z}$ (left) and $\mathbf{S_Y}$ (right) at 40 fs (top row) and 1 ps (bottom row) population time. Gridlines correspond to the exciton energies derived from the cross-peak analysis, and are labeled according to the exciton numbering used in the text.

The excitonic energies extracted from our analysis, listed in Table 1, are generally in good agreement with those derived by simultaneous fits to multiple spectra by Vulto *et al.*[22] We find significant disagreement only in the energy of exciton **6**. The somewhat higher energy derived from their procedure is likely due to the strong overlap of the spectrally broad transitions of excitons **6** and **7**, which are not clearly separable in linear- and transient absorption- spectra, making assignment from fitting of spectra difficult.

In agreement with the spectral structure of the 2D spectra in Figure 1, the cross-peak pattern in the PAS spectra implies an excitonic structure with strong correlation between most transitions. A notable exception is found for the cross-peak correlation pattern of exciton **3**: here a number of high-energy cross-peaks are observed, but above-diagonal cross-peaks with any *lower* energy

excitons are absent, implying spatial separation from the bottom of the FMO energy-ladder. The spatial isolation of this exciton has been theoretically predicted[11] as a result of strong localization of exciton **3** at BChl sites I and II, where the partially overlapping excitons **1-5** (located at BChl sites III, IV, V, and VII) have negligible probability density. This situation is schematically illustrated in Figure 1A.

Close examination of the $\mathbf{S_Y}$ PAS spectrum in Figure 2 reveals two weak off-diagonal features, which appear as (above- and below- diagonal) cross-peaks corresponding to a correlation between exciton **3** and a state in the 12700-12750 cm^{-1} (~785 nm) spectral region. To our knowledge no experimental observation of such a high energy state has been reported, however the estimated energy agrees with the predictions by Busch *et al.*[8] for the exciton localized primarily on the recently discovered BChl 8 (other assignments of the spectral contribution of this exciton can be found in literature, *e.g.* Bina and Blankenship[7]). Following the work of Olbrich *et al.*[9] and Adolphs and Renger[11], the strongest correlation of the high-energy exciton (mostly BChl 8) with exciton **3** implies that it is spatially close to BChl sites I and II, but on the *neighboring* unit in the FMO trimer. While the spectral signature in the PAS maps is clear, we note that the small oscillator strength of this transition, likely due to a very small population of BChl 8 in isolated FMO, renders it as only a minor contributor to the absorption spectrum.

With the exciton energies and their correlations in place, we can now analyze the details of energy transfer through the complex. With increasing population time the downwards flow of energy through FMO is observed as shifting of the SE signal amplitude from the higher-energy diagonal peaks to lower-energy cross-peaks and as lineshape changes. This overall relaxation can be separated into three distinct "stages", characterized by different time scales. The initial *intra*-unit relaxation can be observed as the movement of SE signal from higher energy states to the

lowest exciton **1,** and proceeds on a largely sub-picosecond time scale. After a few picoseconds this transfer is complete, leaving the distinctive "streaked" spectral structure characteristic of shared GSB systems, illustrated by the 2D spectrum at 5 ps population time shown in Figure 1C. However rounding of the initially strongly diagonally elongated lineshapes is fully completed only after approximately 100 ps, indicating a strong memory of initial excitation frequency of the system. These subtle spectral changes can be seen by comparison of the spectra at 5 ps and 1 ns in in Figure 1C. The dynamics of these lineshape changes can be extracted by analysis of decay associated spectra (DAS), where the spectral shape time-evolution appears as a slow component well-separated from *intra*-unit energy transfer processes (see SI for DAS spectra). At 77 K this analysis yields a rate of a few tens of picoseconds for these dynamics, in reasonable agreement with the spectral decay components assigned to *inter*-unit energy transfer in low-temperature spectral hole-burning[19, 37] and pump-probe[38] experiments. Following *intra*-unit energy transfer and lineshape changes, the remaining spectrum decays without further changes on a timescale of nanoseconds, consistent with the fluorescence lifetime (approximately 2 ns, using red-edge excitation[39]).

Quantitative characterization of the individual transfer steps in this highly complex overall relaxation network is challenging. However it can be made tractable, as the observations above approximately reduce the full relaxation dynamics to three independent stages: 1) *intra*-unit relaxation in exciton manifold of seven states 2) *inter*-unit relaxation in an inhomogeneous distribution of "exciton **1** states", and 3) ground state recovery. We focus here in particular on the first *intra*-unit energy transfer processes, as the short time relaxation has been the most challenging for the traditional techniques.

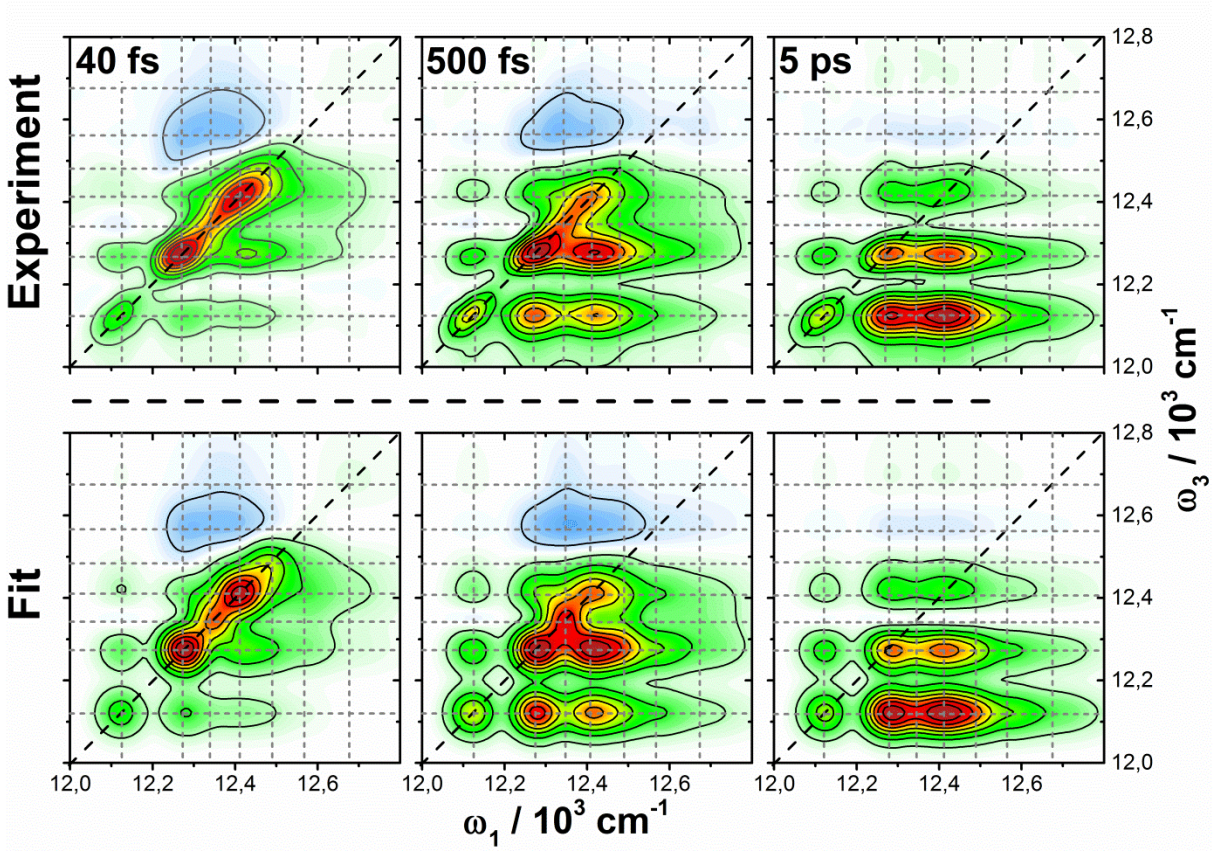

Figure 3: Comparison of normalized experimental 2D spectra (top row) and 2D spectra calculated from the kinetic fit (bottom row) at three population times. Gridlines correspond to the excitonic energy.

2D spectra can essentially be viewed as a two-dimensional matrix of kinetic traces. Such an extensive set of kinetic data obviously lends itself well to global analysis and global fitting approaches. The most common such approach, using decay associated spectra (DAS) of sum-of-exponentials kinetic fits, is comparatively simple and often highly illuminating. It is however only quantitatively useful in systems where the component lifetimes are very well separated[40]. In the case of *intra*-unit relaxation in FMO a large number of transfer processes appear with similar rates, resulting in significant crosstalk between the parameters in a global DAS fit. It thus yields only qualitative information in this time-regime, and only a "collective" sub-ps component

appears, which cannot be reliably separated into its individual constituents (a four-component DAS fit can be found in the SI).

Quantitative analysis of the initial relaxation processes in FMO clearly requires a different approach. Here we take advantage of the detailed knowledge about excitonic state energies and connectivity derived from the PAS spectra to directly impose a realistic physical model to the data. This allows the construction of a set of coupled differential equations, from which the transition rate constants can be extracted directly by fitting to the experimental data. Our routine globally fits GSB+ESA and SE contributions to all points in the 2D spectra simultaneously with the constraint of the assumed model, requiring only the input of the laser spectrum, temperature, number of states, and approximate linewidths as initial conditions. Details of this routine are given in the SI. In order to improve convergence of the fitting procedure we use as starting conditions the exciton energies extracted from the PAS maps, and the assumption that the largest transition rates from a given excitonic level are connected to transitions between spatially overlapping excitons (as seen by the presence of above-diagonal cross-peaks). We further ignore BChl 8 in these fits, as it contributes negligibly to the observed photo-induced dynamics due to its weak absorption. With these starting parameters we can extract all state-to-state transfer rates by a simultaneous fit of the 2D spectra at all population times with reproduction of the LA spectrum as an additional constraint. Comparison between a few experimental 2D spectra and spectra extracted from the fit are shown in Figure 3, and the resulting model is summarized in the transition matrix in Table 1 and the schematic illustration in Figure 4.

Table 1: Energy transfer rates between excitonic states

	|7⟩	**|6⟩**	**|5⟩**	**|4⟩**	**|3⟩**	**|2⟩**	E_n
|7⟩	**-29.9**	-	-	-	-	-	12.67
|6⟩	1.4	**-16.4**	-	-	-	-	12.57
|5⟩	6.4	-	**-5.1**	-	-	-	12.48
|4⟩	16.0	7.6	1.5	**-3.9**	-	-	12.41
|3⟩	6.1	2.4	1.2	-	**-0.83**	-	12.34
|2⟩	-	6.2	2.2	1.6	0.65	**-2.7**	12.27
|1⟩	-	-	-	1.3	-	2.3	12.12

Transfer rates (population decay negative, population grow-in positive) in units of ps^{-1}. Upwards transfer rates and rates contributing <5% of the level decay are omitted for clarity. Energies of the excitons (in 10^3 cm^{-1}) are found in the right-most column of the corresponding row.

The rates extracted here agree qualitatively with those determined in transient absorption experiments[20-22, 28], in that *intra*-unit energy transfer is found to proceed largely on sub-picosecond timescales and that higher energy excitons are extremely short lived. However, accurate kinetics have not been available from these earlier studies, as the exciton lifetimes are comparable to- or shorter- than the excitation pulses used in several cases. Further, deconvolution of the observed decays into individual energy transfer steps could not be easily effected due to the large number of transitions necessarily covered by the finite-width laser spectra. Both these issues are circumvented in 2DES, which lets us to use pulses that are substantially shorter than the exciton lifetimes, and to observe the level-to-level transfer times directly in the cross-peak dynamics. While 2DES literature on FMO is substantial, so far these highly advantageous characteristics have not been used for quantitative experimental characterization of the energy transfer network in FMO.

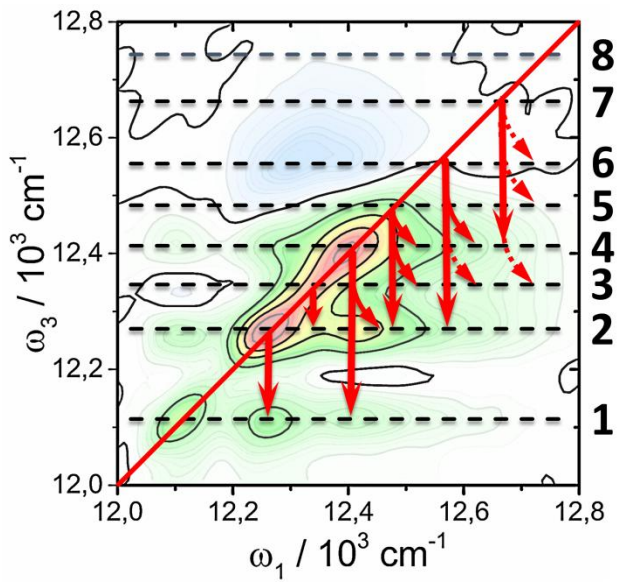

Figure 4: 2D spectrum at 100 fs delay with excitonic levels indicated with dashed lines. A schematic illustration of the relaxation cascade is inserted. Solid arrows indicate channels responsible for a large relative fraction of the total transfer from a given level, while dashed arrows indicate minor channels.

As illustrated in Figure 4 and Table 1 it is apparent that there is some "branching" in the relaxation, in that *e.g.* exciton **6** preferentially relaxes *via* exciton **4** and not **5**. Overall however we observe a complex and strongly interconnected relaxation process. While it is clear that the spatial overlap of excitons influence the magnitude of individual transition rates in the relaxation, our data do not support the model of two spatially separated relaxation pathways through the complex suggested in early 2DES work[12, 27, 41]. Instead we observe a "multi-branching", interconnected network of transfer pathways where each state may transfer its population into a number of other states. The discrepancy between the extracted models likely originates from the qualitative nature of earlier 2DES work on population dynamics, where only a select few "snapshots" of the population decay was measured.

An exception to the otherwise rapid *intra*-unit dynamics is the picosecond timescale relaxation of exciton **3**. Transfer to this state from other states occurs with relatively low probability and de-population is slow, thus it poses as "semi-trap" in the otherwise fast and efficient energy transfer network. The weak connection of this exciton to the rest can be understood from the lack of correlation with lower energy states in the "energy ladder". This implies some degree of spatial isolation from its energetically favorable decay channels, in agreement with earlier calculations[11], which in turn intuitively suggests a smaller relaxation rate. Though this slow kinetic component has been observed in transient absorption kinetics[22, 42], the significance of such a trap to the operation of native FMO is unclear. The relatively low probability of population and slow deactivation implies a minor, if any, role in the function of the complex.

The *inter*-unit energy transfer, apparent in the lineshape dynamics after completion of the initial relaxation to exciton **1,** appear simply as an additional component in the kinetic traces at long times. It was however omitted here for clarity. Regardless of whether the rate of this process is extracted by lineshape changes, DAS, or rate constant fitting, it appears with a rate constant of approximately 3.5×10^{-2} ps^{-1}, in qualitative agreement with *inter*-unit energy transfer rates estimated from liquid helium temperature spectral hole-burning[19, 37] and pump-probe measurements[38].

In summary we have shown that the high spectral- and temporal- resolution of 2DES in combination with a decomposition of the total spectrum into orthogonal PAS maps allows emerging of a complete and consistent picture of both the electronic structure and the energy transfer kinetics in FMO at low temperatures. The selective suppression of the strongly "diagonal" spectral contributions further allowed the first experimental observation of the exciton primarily situated on the recently discovered elusive BChl 8. Further, we demonstrate

that the large amount of spectrally well-resolved kinetic data inherently present in a typical 2DES dataset forms an ideal basis for advanced global fitting procedures. The complex, inter-connected seven-state relaxation in FMO was thus resolved into a matrix of level-to-level transfer rates by use of an in-house developed fitting tool. This resulting transfer matrix of multi-branching pathways represents a considerable refinement to the present model of the excited state relaxation in FMO. Finally we note that the approach of direct-fitting-of-rates to sets of 2DES and LA spectra taken here is general, and can be applied to a wide array of systems where exponential kinetics models are applicable. In particular this can prove beneficial in the analysis of complex systems, where ambiguities in fits of pump-probe data may hinder the construction of a reliable and meaningful physical model of the relaxation dynamics.

Experimental Section

Details on bacteria culture growth and FMO isolation procedures are given in the SI.

All measurements were done in a standard cryogenic buffer containing a 1:2 ration of aqueous buffer: glycerol. The sample was kept in a demountable 0.5 mm pathlength fused silica cell, supported in a temperature controlled liquid nitrogen bath cryostat (Optistat DN2, Oxford Instruments) equipped with fused silica windows. The maximum optical density in the probed spectral window was kept between 0.1 and 0.3 in all experiments. Linear absorption spectra were recorded, in the cryostat, on a Perkin-Elmer lambda 1050 UV/Vis/NIR spectrometer.

The 2DES setup is described in detail elsewhere[43], we briefly summarize key points here: A 1027 nm centered Pharos (Light Conversion ltd.) laser is used to pump a non-collinear optical amplifier (Light Conversion ltd.), the output of which is compressed by a fused silica prism compressor. The resulting output is approximately 14 fs, ~80 nm FWHM pulses with a spectrum centered at 805 nm. The pulse energy was 1.5 nJ or 750 nJ, and the experiment was done at 5

kHz repetition rate. The coherence time was scanned from -270 to +450 fs in 1.8 fs steps, resulting in a spectral resolution of 37 cm^{-1} on the ω_1 axis.

To avoid depolarization artifacts in the population dynamics we record spectra at the magic angle polarization conditions ⟨54.7,54.7,0,0⟩. Here each number corresponds to the polarization angle of the three exciting pulses and analyzer. Additional spectra were recorded with ⟨0,0,0,0⟩ and ⟨90,90,0,0⟩ polarization conditions to generate PAS spectra. Proper phase of the measured 2D spectra were in all cases determined by comparison of 2D projection with pump-probe spectra recorded under the same conditions[23]. 2DES spectra are recorded at a range of population times over several measurement series, with a typical series containing 50-100 2D spectra. The total measured population times span the range from 0 fs to 1 ns. We assess the quality of the 2D spectra by extracting transient absorption spectra and comparing this with literature data. Overall we find good agreement. During the acquisition we observed slight selective bleaching of exciton 2, which necessitated the use of low-intensity pulses and low repetition rates. Careful control of the conditions let us keep the bleaching of this peak <5% over a 120 population time point measurement, while the bleaching was negligible during the exciton 2 lifetime.

Kinetic analysis was done by simultaneous fitting the kinetics in all points in the 2DES map, using a combination of the Marquart-Levenberg algorithm and particle swarm optimization. The quality of the fits were assessed by χ^2 analysis and visual comparison of the extracted 2DES and LA spectra with their experimental counterparts. For more details see SI.

Supporting Information Available

FMO extraction procedures, high-cryogenic temperature 2D spectra, details on PAS generation, 2D-DAS spectra, details on fitting procedure. This information can be found on the internet at http://pubs.acs.org.

Notes

The authors declare no competing financial interests.

Acknowledgements

E.T., K.Z., and D.Z. acknowledges support from the Knut & Alice Wallenberg foundation and Swedish Research Council. D.B. acknowledges support by Czech Science Foundation under grant number P501/12/G055 and institutional support RVO:60077344. J.D. thanks the DFG for funding within the Research Unit "Light-induced dynamics in molecular aggregates" (FOR1809).

References

(1) Fenna, R. E.; Matthews, B. W. Chlorophyll Arrangement in a Bacteriochlorophyll Protein from Chlorobium-Limicola. *Nature* **1975,** *258*, 573-577.

(2) Tronrud, D. E.; Wen, J. Z.; Gay, L.; Blankenship, R. E. The Structural Basis for the Difference in Absorbance Spectra for the Fmo Antenna Protein from Various Green Sulfur Bacteria. *Photosynth. Res.* **2009,** *100*, 79-87.

(3) Milder, M. T. W.; Bruggemann, B.; van Grondelle, R.; Herek, J. L. Revisiting the Optical Properties of the Fmo Protein. *Photosynth. Res.* **2010,** *104*, 257-274.

(4) Savikhin, S.; Buck, D. R.; Struve, W. S. Oscillating Anisotropies in a Bacteriochlorophyll Protein: Evidence for Quantum Beating between Exciton Levels. *Chem. Phys.* **1997,** *223*, 303-312.

(5) Engel, G. S.; Calhoun, T. R.; Read, E. L.; Ahn, T. K.; Mancal, T.; Cheng, Y. C.; Blankenship, R. E.; Fleming, G. R. Evidence for Wavelike Energy Transfer through Quantum Coherence in Photosynthetic Systems. *Nature* **2007,** *446*, 782-786.

(6) Panitchayangkoon, G.; Hayes, D.; Fransted, K. A.; Caram, J. R.; Harel, E.; Wen, J. Z.; Blankenship, R. E.; Engel, G. S. Long-Lived Quantum Coherence in Photosynthetic Complexes at Physiological Temperature. *Proc. Natl. Acad. Sci. U.S.A.* **2010,** *107*, 12766-12770.

(7) Bina, D.; Blankenship, R. E. Chemical Oxidation of the Fmo Antenna Protein from Chlorobaculum Tepidum. *Photosynth. Res.* **2013,** *116*, 11-19.

(8) Busch, M. S. A.; Muh, F.; Madjet, M. E.; Renger, T. The Eighth Bacteriochlorophyll Completes the Excitation Energy Funnel in the Fmo Protein. *J. Phys. Chem. Lett.* **2011,** *2*, 93-98.

(9) Olbrich, C.; Jansen, T. L. C.; Liebers, J.; Aghtar, M.; Strumpfer, J.; Schulten, K.; Knoester, J.; Kleinekathofer, U. From Atomistic Modeling to Excitation Transfer and Two-Dimensional Spectra of the Fmo Light-Harvesting Complex. *J. Phys. Chem. B* **2011,** *115*, 8609-8621.

(10) Olbrich, C.; Strumpfer, J.; Schulten, K.; Kleinekathofer, U. Theory and Simulation of the Environmental Effects on Fmo Electronic Transitions. *J. Phys. Chem. Lett.* **2011,** *2*, 1771-1776.

(11) Adolphs, J.; Renger, T. How Proteins Trigger Excitation Energy Transfer in the Fmo Complex of Green Sulfur Bacteria. *Biophys. J.* **2006,** *91*, 2778-2797.

(12) Cho, M. H.; Vaswani, H. M.; Brixner, T.; Stenger, J.; Fleming, G. R. Exciton Analysis in 2d Electronic Spectroscopy. *J. Phys. Chem. B* **2005,** *109*, 10542-10556.

(13) Vulto, S. I. E.; de Baat, M. A.; Louwe, R. J. W.; Permentier, H. P.; Neef, T.; Miller, M.; van Amerongen, H.; Aartsma, T. J. Exciton Simulations of Optical Spectra of the Fmo Complex from the Green Sulfur Bacterium Chlorobium Tepidum at 6 K. *J. Phys. Chem. B* **1998,** *102*, 9577-9582.

(14) Ratsep, M.; Cai, Z. L.; Reimers, J. R.; Freiberg, A. Demonstration and Interpretation of Significant Asymmetry in the Low-Resolution and High-Resolution Q(Y) Fluorescence and Absorption Spectra of Bacteriochlorophyll A. *J. Chem. Phys.* **2011,** *134*, 024506.

(15) Louwe, R. J. W.; Vrieze, J.; Hoff, A. J.; Aartsma, T. J. Toward an Integral Interpretation of the Optical Steady-State Spectra of the Fmo-Complex of Prosthecochloris Aestuarii. 2. Exciton Simulations. *J. Phys. Chem. B* **1997,** *101*, 11280-11287.

(16) Pearlstein, R. M. Theory of the Optical-Spectra of the Bacteriochlorophyll-a Antenna Protein Trimer from Prosthecochloris-Aestuarii. *Photosynth. Res.* **1992,** *31*, 213-226.

(17) Wendling, M.; Przyjalgowski, M. A.; Gulen, D.; Vulto, S. I. E.; Aartsma, T. J.; van Grondelle, R.; van Amerongen, H. The Quantitative Relationship between Structure and Polarized Spectroscopy in the Fmo Complex of Prosthecochloris Aestuarii: Refining Experiments and Simulations. *Photosynth. Res.* **2002,** *71*, 99-123.

(18) Franken, E. M.; Neerken, S.; Louwe, R. J. W.; Amesz, J.; Aartsma, T. J. A Permanent Hole Burning Study of the Fmo Antenna Complex of the Green Sulfur Bacterium Prosthecochloris Aestuarii. *Biochemistry* **1998,** *37*, 5046-5051.

(19) Ratsep, M.; Blankenship, R. E.; Small, G. J. Energy Transfer and Spectral Dynamics of the Three Lowest Energy Q(Y)-States of the Fenna-Matthews-Olson Antenna Complex. *J. Phys. Chem. B* **1999,** *103*, 5736-5741.

(20) Savikhin, S.; Struve, W. S. Ultrafast Energy-Transfer in Fmo Trimers from the Green Bacterium Chlorobium-Tepidum. *Biochemistry* **1994,** *33*, 11200-11208.

(21) Buck, D. R.; Savikhin, S.; Struve, W. S. Ultrafast Absorption Difference Spectra of the Fenna-Matthews-Olson Protein at 19 K: Experiment and Simulations. *Biophys. J.* **1997,** *72*, 24-36.

(22) Vulto, S. I. E.; de Baat, M. A.; Neerken, S.; Nowak, F. R.; van Amerongen, H.; Amesz, J.; Aartsma, T. J. Excited State Dynamics in Fmo Antenna Complexes from Photosynthetic Green Sulfur Bacteria: A Kinetic Model. *J. Phys. Chem. B* **1999,** *103*, 8153-8161.

(23) Jonas, D. M. Two-Dimensional Femtosecond Spectroscopy. *Annu. Rev. Phys. Chem.* **2003,** *54*, 425-463.

(24) Mukamel, S. Multidimensional Femtosecond Correlation Spectroscopies of Electronic and Vibrational Excitations. *Annu. Rev. Phys. Chem.* **2000,** *51*, 691-729.

(25) Hybl, J. D.; Albrecht, A. W.; Faeder, S. M. G.; Jonas, D. M. Two-Dimensional Electronic Spectroscopy. *Chem. Phys. Lett.* **1998,** *297*, 307-313.

(26) Hybl, J. D.; Ferro, A. A.; Jonas, D. M. Two-Dimensional Fourier Transform Electronic Spectroscopy. *J. Chem. Phys.* **2001,** *115*, 6606-6622.

(27) Brixner, T.; Stenger, J.; Vaswani, H. M.; Cho, M.; Blankenship, R. E.; Fleming, G. R. Two-Dimensional Spectroscopy of Electronic Couplings in Photosynthesis. *Nature* **2005,** *434*, 625-628.

(28) Vulto, S. I. E.; Neerken, S.; Louwe, R. J. W.; de Baat, M. A.; Amesz, J.; Aartsma, T. J. Excited-State Structure and Dynamics in Fmo Antenna Complexes from Photosynthetic Green Sulfur Bacteria. *J. Phys. Chem. B* **1998,** *102*, 10630-10635.

(29) Thulstrup, E. W.; Eggers, J. H. Moment Directions of the Electronic Transitions of Fluoranthene. *Chem. Phys. Lett.* **1968,** *1*, 690-692.

(30) Michl, J.; Thulstrup, E. W. Ultraviolet and Infrared Linear Dichroism - Polarized-Light as a Probe of Molecular and Electronic-Structure. *Acc. Chem. Res.* **1987,** *20*, 192-199.

(31) Valeur, B.; Weber, G. Resolution of Fluorescence Excitation Spectrum of Indole into 1la and 1lh Excitation Bands. *Photochem. Photobiol.* **1977,** *25*, 441-444.

(32) Albrecht, A. C. Polarizations and Assignments of Transitions - Method of Photoselection. *J. Mol. Spectrosc.* **1961,** *6*, 84-104.

(33) Thyrhaug, E.; Sorensen, T. J.; Gryczynski, I.; Gryczynski, Z.; Laursen, B. W. Polarization and Symmetry of Electronic Transitions in Long Fluorescence Lifetime Triangulenium Dyes. *J. Phys. Chem. A* **2013,** *117*, 2160-2168.

(34) Zanni, M. T.; Ge, N. H.; Kim, Y. S.; Hochstrasser, R. M. Two-Dimensional Ir Spectroscopy Can Be Designed to Eliminate the Diagonal Peaks and Expose Only the Crosspeaks Needed for Structure Determination. *Proc. Natl. Acad. Sci. U.S.A.* **2001,** *98*, 11265-11270.

(35) Abramavicius, D.; Voronine, D. V.; Mukamel, S. Unravelling Coherent Dynamics and Energy Dissipation in Photosynthetic Complexes by 2d Spectroscopy. *Biophys. J.* **2008,** *94*, 3613-3619.

(36) Read, E. L.; Engel, G. S.; Calhoun, T. R.; Mancal, T.; Ahn, T. K.; Blankenship, R. E.; Fleming, G. R. Cross-Peak-Specific Two-Dimensional Electronic Spectroscopy. *Proc. Natl. Acad. Sci. U.S.A.* **2007,** *104*, 14203-14208.

(37) Kell, A.; Acharya, K.; Zazubovich, V.; Jankowiak, R. On the Controversial Nature of the 825 Nm Exciton Band in the Fmo Protein Complex. *J. Phys. Chem. Lett.* **2014,** *5*, 1450-1456.

(38) Vulto, S. I. E.; Streltsov, A. M.; Aartsma, T. J. Excited State Energy Relaxation in the Fmo Complexes of the Green Bacterium Prosthecochloris Aestuarii at Low Temperatures. *J. Phys. Chem. B* **1997,** *101*, 4845-4850.

(39) Zhou, W. L.; Lobrutto, R.; Lin, S.; Blankenship, R. E. Redox Effects on the Bacteriochlorophyll a-Containing Fenna-Matthews-Olson Protein from Chlorobium-Tepidum. *Photosynth. Res.* **1994,** *41*, 89-96.

(40) van Stokkum, I. H. M.; Larsen, D. S.; van Grondelle, R. Global and Target Analysis of Time-Resolved Spectra. *BBA-Bioenergetics* **2004,** *1657*, 82-104.

(41) Read, E. L.; Schlau-Cohen, G. S.; Engel, G. S.; Wen, J. Z.; Blankenship, R. E.; Fleming, G. R. Visualization of Excitonic Structure in the Fenna-Matthews-Olson Photosynthetic Complex by Polarization-Dependent Two-Dimensional Electronic Spectroscopy. *Biophys. J.* **2008,** *95*, 847-856.

(42) Savikhin, S.; Buck, D. R.; Struve, W. S. Toward Level-to-Level Energy Transfers in Photosynthesis: The Fenna-Matthews-Olson Protein. *J. Phys. Chem. B* **1998,** *102*, 5556-5565.

(43) Augulis, R.; Zigmantas, D. Two-Dimensional Electronic Spectroscopy with Double Modulation Lock-in Detection: Enhancement of Sensitivity and Noise Resistance. *Opt. Express* **2011,** *19*, 13126-13133.

Supporting Information: Exciton Structure and Energy Transfer in the Fenna-Matthews-Olson Complex

Erling Thyrhaug[1], Karel Žídek[1], Jakub Dostál[1,2], David Bína[3], Donatas Zigmantas[1].*

[1] - Department of Chemical Physics, Lund University, P.O. Box 124, 22100 Lund, Sweden

[2] - Institut für Physikalische und Theoretische Chemie, Universität Würzburg, Am Hubland, D-97074 Würzburg, Germany

[3] - Biology Centre CAS, Branišovská 31, and Faculty of Science, University of South Bohemia, Branišovská 1760, 370 05 České Budějovice, Czech Republic

Corresponding Author

* donatas.zigmantas@chemphys.lu.se

C. tepidum culture and FMO preparation: Cultivation of *C. tepidum* (strain TLS, DSM 12025) was performed in 800 mL batches of modified Pfennig medium (Wahlund et al.[1]) kept at 45°C, continuously illuminated with 60 W incandescent light bulbs. FMO preparation was based on Wen et al.[2] Briefly, cells were harvested after 3 days of cultivation by centrifugation at 6000 g, resuspended in 20 mM Tris-HCl, pH 8 and broken using EmulsiFlex-C5 (Avestin Inc., Canada) at 20000 psi. Following removal of unbroken cells by low speed centrifugation the membranes were collected by ultracentrifugation at 200000 g for 2 hours. FMO was released from membranes using 0.4 M Na_2CO_3 added in two steps over the course of 2 days. Following removal of debris by ultracentrifugation, the soluble protein fraction was dialyzed against 20 mM Tris, pH 8 for 72 hours, concentrated and purified using size exclusion and anion exchange chromatography until the OD_{271} / OD_{371} ratio dropped under ~0.6.

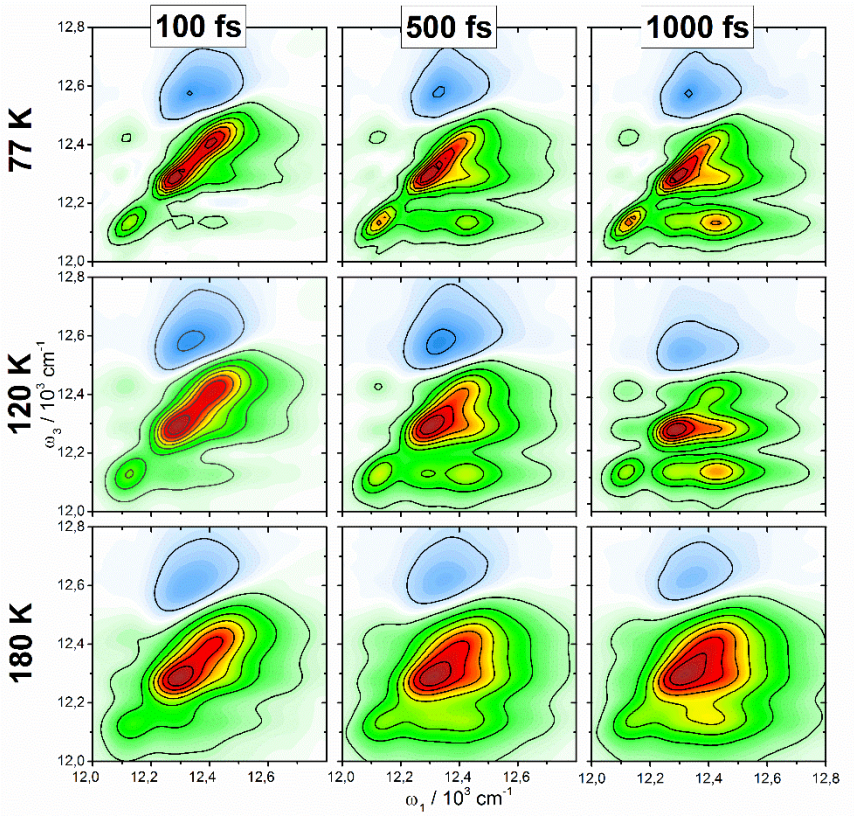

Figure S 1: Comparison of 2DES spectra, measured with magic angle polarization settings at different population times and temperatures.

Comparison of different approaches to PAS generation: Several different approaches can be found to separate fluorescence, pump-probe, or 2D spectrum into polarized components, thus allowing for the removal of unwanted signals (or at the very least – maximization of the desired signal). We are aware of at least three (for the present case) functionally similar, but conceptually different approaches to spectral decomposition into polarization associated spectra (PAS). These are: the anisotropy/PAS approach of Albrecht[3], the polarization tensor equation for four-wave mixing of Wright[4] and Hochstrasser[5-6], and the symmetry approach of Abramavicious & Mukamel[7]. These lead in many cases to (within a sign difference) identical results, as fundamentally the same operations are applied to the experimental data. In analysis of incoherent

dynamics and static excitonic structure (as is the case in this study), we favor the Albrecht approach due to its straightforward geometric interpretation. It is however worth noting some conceptual differences in the different approaches.

The Albrecht approach separates the isotropic spectrum (by use of the fundamental fluorescence-, pump-probe-, or 2DES- anisotropy) into components belonging to orthogonal molecular axes. In practice the absorptive contributions parallel and perpendicular to the probed transition (i.e. emission or pump-probe detected signal) are extracted. In the original paper an isotropic ensemble and orthogonal transitions were assumed.[3] Neither are fundamental limitations, and generalization to oriented ensembles and non-orthogonal transitions are straightforward, though somewhat cumbersome. In ultrafast- and multi-dimensional-spectroscopy two major limitations appear: 1) working via the fundamental anisotropy, only pulse sequences with pairwise identical pulses can be treated. This only arise as an issue in specific 2DES (and possibly in other multidimensional techniques) pulse-polarization sequences, as this requirement is automatically fulfilled for e.g. fluorescence and transient absorption. 2) Coherent signals do not appear in the theory. If coherences are induced by the experiment, these appear in the PAS spectra, however no direct interpretation of these quantum beats is provided. In the PAS spectra used in the main text pure correlated vibrational coherences (in the language of Jonas and coworkers[8]) will be suppressed in the S_Y spectrum, while electronic or vibronically mixed coherences between states of different polarization will appear as (off-phase) beatings between the two PAS spectra.

The approach by Abramavicious and Mukamel exploits certain symmetries (at time = 0) between pulse sequences in 2D experiments to cancel or enhance specific signals. This is clearly convenient for identifying spectral combinations that provides the desired type of signal, e.g. to

maximize coherent or chiral signals. No geometric information is provided however, and the approach may thus be inconvenient for exciton structure characterization.

In Hochstrassers' and Wright's approach all relevant information is collected in a tensor equation. This allows one to directly calculate the signal in a given "pixel" in the 2DES map, given the contributing transition moments and the polarization of the optical pulses. While this is a completely general approach, it does not in general provide any straight-forward method for identifying polarization conditions or combination spectra that maximizes (or minimizes) a given signal. To do so one must solve the tensor equation directly, which may not lead to the most straight-forward or elegant solution, depending on the problem at hand. Further it is a "point-by-point" calculation approach, and thus reveals little about the spatial relations in complex exciton structures.

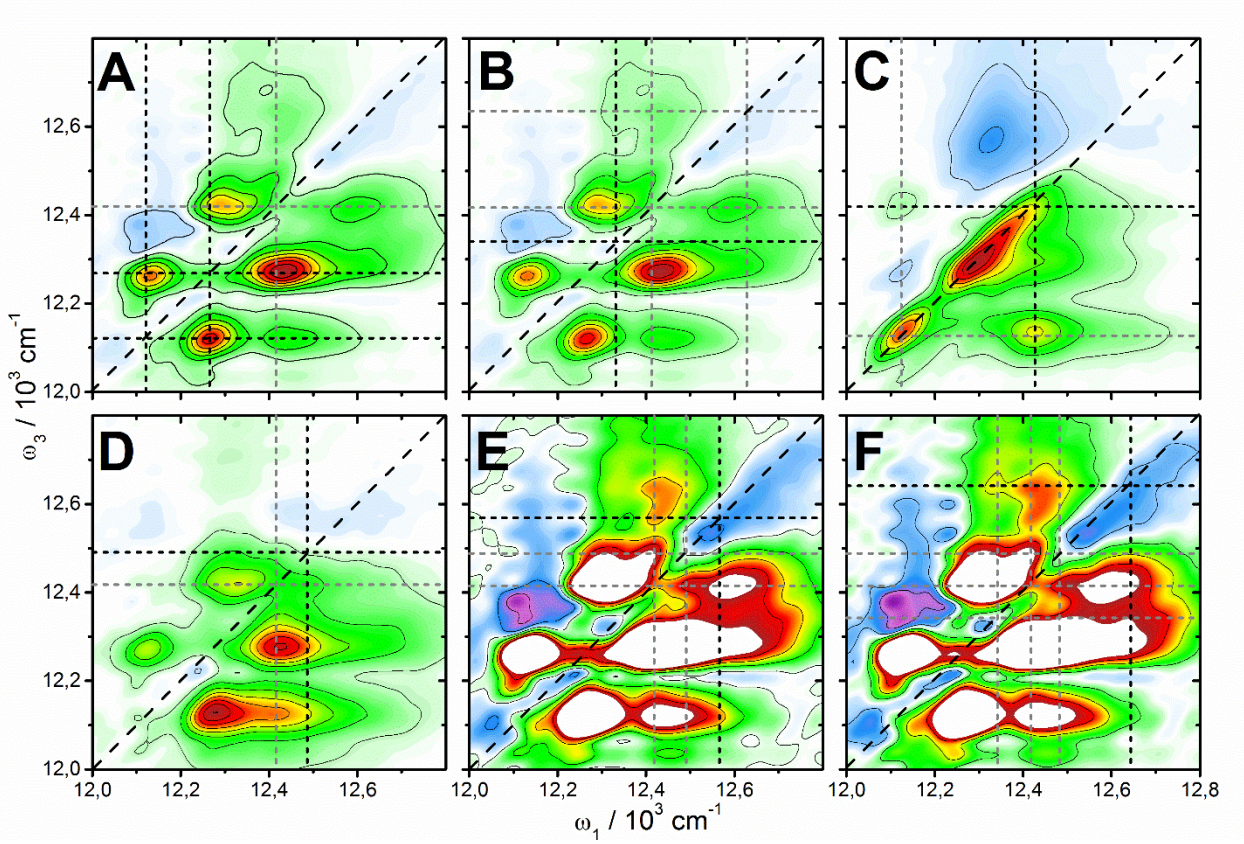

Figure S 2: Examples of energy-level triangulations in PAS maps. Panels A, B, E and F: S_Y spectrum at 40 fs population time. Panel C: S_Z spectrum at 1 ps population time. Panel D: S_Y spectrum at 1 ps population time. Amplitude is rescaled in Panels E and F to better reveal the cross-peaks. A: excitons 1 and 2 (black lines) and exciton 4 (gray). B: Exciton 3 (black) and excitons 4 and 6 (gray). C: Exciton 4 (black) and exciton 1 (gray). D: Exciton 5 (black) and exciton 4 (gray). E: Exciton 6 (black) and excitons 4 and 5 (gray). F: Exciton 7 (black) and excitons 3-5 (gray).

Table S 1: Comparison of exciton energies with literature data

Exciton	Current Work - PAS	Current Work - Fit	Vulto *et al.*
1	12.12	12.121	12.113
2	12.27	12.275	12.262
3	12.34	12.348	12.355
4	12.41	12.415	12.414
5	12.48	12.487	12.448
6	12.57	12.581	12.611
7	12.64	12.685	12.649

Exciton energies as read from PAS spectra, after kinetic fit, and literature values from Vulto and coworkers[9]. Energies in 10^3 cm^{-1}. The second data column, with energies resulting from the kinetic fit, represent a refinement of the exciton energies estimated by visual inspection in the first data column.

DAS Analysis: A four-component sum-of-exponential DAS decomposition of the 2DES data is shown in Figure S 3. The two longest components are well separated, and DAS analysis provides reliable decay rates and spectral shapes. These components have been assigned to inter-unit energy transfer and the ground-state recovery respectively. The 1.2 ps component is similarly relatively well captured by DAS, mainly showing the decay of exciton 3 (and an associated above-diagonal excited state absorption band) and the corresponding rise of the population of exciton 1. The remaining dynamics that are necessary to capture are the numerous intra-unit transfer processes, which have relatively closely spaced rates. This is demonstrated in the short-lifetime DAS in Figure S 3, where a large number of components appear with an identical lifetime of 200 fs. Adding more decay-components (without more advanced analysis approaches) in order to capture the individual transfer processes does not result in a meaningful

improvement in the fit statistics. In order to extract the individual level-to-level transfer rates rather than the sum-total observed in DAS we thus fit the data directly to a kinetic model.

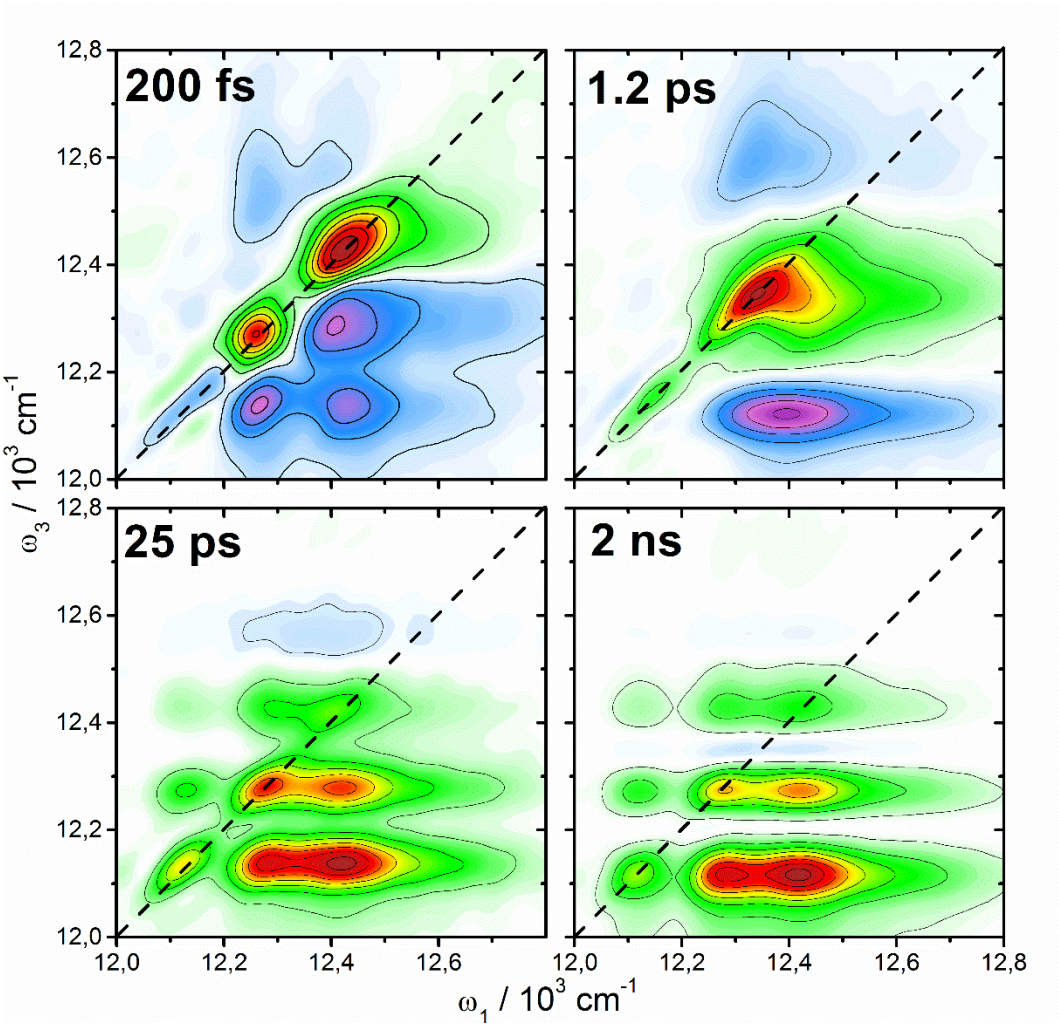

Figure S 3: Four-component DAS fit of magic angle data at 77 K. The components corresponding to the relaxation of exciton 3 (1.2 ps here), inter-unit energy transfer (25 ps) and ground-state recovery (~2 ns) are well-defined due to large separation in apparent lifetimes. The remaining intra-unit transfer processes appear as a single 200 fs component due to presence of multiple relaxation processes with similar lifetimes.

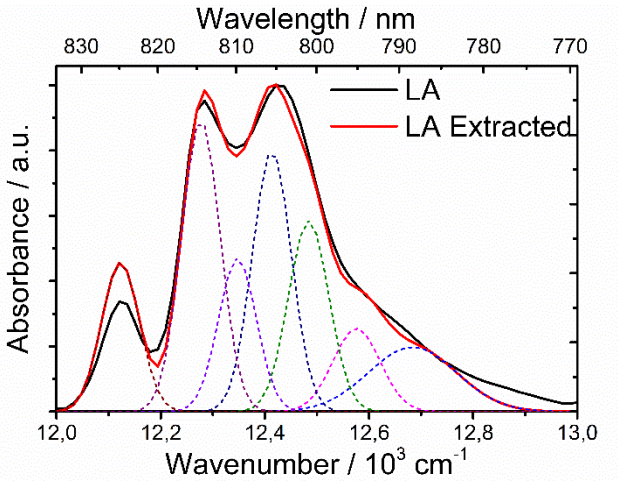

Figure S 4: Linear absorption spectrum (black) and LA spectrum calculated from the kinetic fit (red). Excitonic transitions contributing to the kinetic fit shown as dashed lines.

Fitting Procedure: The dynamics resolved by transient absorption (TA) spectroscopy is most often interpreted in terms of a rate equation model. The assumptions are made that 1: the decay of the population of one particular excited state (transient species) i is directly proportional to the population itself and 2: that the population of this state is increased by the population transfer from the other states $j \neq i$, which is seen as a decay of these states. The connectivity between N species and one ground state is described by a set of "intrinsic rate constants" k_{ij}. The mathematical formulation of this model is then a set of homogeneous linear differential equations of the first order

$$\frac{\mathrm{d}\vec{p}(t)}{\mathrm{d}t} = K\vec{p}(t), \qquad \text{(S1)}$$

where $\vec{p}(t)$ is (N+1)-component time-dependent vector of populations of individual states. K is a matrix with intrinsic rate constants as its off-diagonal elements. The diagonal elements of K are the "apparent rates" $k_{ii} = -\sum_{j \neq i} k_{ji}$ describing the lifetime of the individual states. As a consequence, the time-evolution of any state can (in almost all cases) be written as a linear combination of exponential functions decaying with different apparent rate constants.

Global analysis – one of the most common method of processing TA spectra – heavily relies on such a formulation. By fitting a set of decaying exponentials at each point of the acquired TA map one can retrieve most prominent apparent rates. By looking at their amplitude distribution in the spectrum one can interpret the spectra of individual states and infer intrinsic rate constants of the transfer processes connecting them. As it has been repeatedly shown before,[10] TA spectra unfortunately do not contain enough information to allow for unambiguous interpretation, since an infinite number of model schemes (combinations of intrinsic rates with spectra of individual states) result in an identical overall evolution of the TA spectrum.

The situation is however different for the 2DES data, because the extra dimension in the absorptive 2D spectra provide necessary additional information, and as a result not every model scheme leading to identical TA spectra generates identical 2D spectra. Therefore, careful analysis of the absorptive 2D spectra can be used to exclude multiple model schemes that would be otherwise considered as a valid interpretation of the TA spectra.

The spectral decomposition used in this paper proceeds as follows. The initial energy of the levels (relative to the ground state - GS), the transition dipole moments, homogeneous linewidths and all downwards rate constants are guessed. Spectral species are constructed as described in detail below. The upwards rate constants are calculated as $k_{up} = k_{down} \cdot \exp(-\Delta E/k_b T)$ to fulfil the detailed balance condition (ΔE is the energy difference between the two states connected by the rate constants, k_b is the Boltzmann constant, and T the absolute temperature). The rate equations are solved numerically using a combination of the classical Runge-Kutta and implicit Euler methods. Multiple initial conditions are used, depending on the excitation wavelength, each time a single state is populated (one spectral species). The subsequent time evolution describes dynamics observed in a single column of the 2D spectrum at the excitation frequency ω_1. The

intensity of each column is further multiplied by the corresponding square of the transition dipole moment to correct for the relative intensities of individual transitions.

The 2D spectral shape of every transient spectral species is assumed to consist of a set of two-dimensional Gaussian bands, arranged in a column and centered at the ω_3 frequencies of the individual states. The amplitude of individual bands is yet to be determined and can be both positive (to reflect the GSB and SE contributions) and negative (ESA contributions). In the fit multiple spectral species can contribute to each column, when multiple states are populated with increasing population time, depending on the energy relaxation pathways.

Altogether the fitted model function S can be written as

$$S = L_3 \,\mathrm{diag}(\mu_i^2)\, F \exp(K' t)\, \mathrm{diag}(\mu_i^2)\, L_1^{\mathrm{T}}, \qquad \text{(S2)}$$

where K' is a (N x N) matrix constructed from the rate constant matrix K by omitting the row and column of rates to or from the ground state. The symbol exp() denotes a matrix exponential. $\mathrm{diag}(\mu_i^2)$ is a diagonal matrix containing squares of transition dipole moments of individual excited states as its non-zero elements. The composition of spectra associated to the individual transient species as a set of Gaussian bands (as described above) is characterized by the matrix product $\mathrm{diag}(\mu_i^2)\, F$. Each element $\mu_{ii}^2 f_{ij}$ (i, j = 1...N) of the matrix product determines the amplitude of the Gaussian band centered at the energy of species i appearing in the spectrum associated to the species j. Matrices $L_1 \in \mathbf{R}^{n_1 \mathrm{x} N}$ and $L_3 \in \mathbf{R}^{n_3 \mathrm{x} N}$ are convolution matrices defining the appearance of individual transitions as 2D Gaussian bands in the actual 2D spectrum containing n_1 and n_3 samples along excitation an detection axis, respectively.

Note that this model cannot properly describe the ESA signal appearing outside the grid of considered states or substantially Stokes-shifted SE. The linewidth of the individual bands is given by the initially guessed homogeneous width, convolved with lifetime broadening,

determined from the rate constants. The unknown amplitudes of individual Gaussian bands of every spectral species are chosen in such a way that the resulting calculated 2D spectrum approximates the experimental data the best. Since the band intensities are linear parameters of the model their best values are uniquely determined from the experimental data by the linear least-square fitting method. Note that a perfect match between the experimental and calculated spectra would still require correct guess of the non-linear parameters (rates, energies, dipole moments and homogeneous linewidths).

The linear absorption spectrum is calculated from the energy levels, dipole moments and linewidths. Fit to the experimental absorption are used as an additional criterion determining the goodness of the fit.

In the following steps all the non-linear parameters are systematically scanned in order to fit the experimental data as well as possible. This is done by a combination of a variant of the particle swarm optimization[11] with Levenberg-Marquardt algorithm. Note that the separation of parameters into linear and non-linear, where the former are determined with respect to the latter is the principle of the variable projections method.[12]

The fitting algorithm was implemented in C++ using Armadillo linear algebra library. The detailed description of the model together with its mathematical properties will be summarized in a separate forthcoming publication.

References

(1) Wahlund, T. M.; Woese, C. R.; Castenholz, R. W.; Madigan, M. T. A Thermophilic Green Sulfur Bacterium from New-Zealand Hot-Springs, Chlorobium-Tepidum Sp-Nov. *Arch. Microbiol.* **1991,** *156*, 81-90.

(2) Wen, J. Z.; Zhang, H.; Gross, M. L.; Blankenship, R. E. Membrane Orientation of the Fmo Antenna Protein from Chlorobaculum Tepidum as Determined by Mass Spectrometry-Based Footprinting. *Proc. Natl. Acad. Sci. U.S.A.* **2009,** *106*, 6134-6139.

(3) Albrecht, A. C. Polarizations and Assignments of Transitions - Method of Photoselection. *J. Mol. Spectrosc.* **1961,** *6*, 84-108.

(4) Zilian, A.; Wright, J. C. Polarization Effects in Four-Wave Mixing of Isotropic Samples. *Mol. Phys.* **1996,** *87*, 1261-1271.

(5) Hochstrasser, R. M. Two-Dimensional Ir-Spectroscopy: Polarization Anisotropy Effects. *Chem. Phys.* **2001,** *266*, 273-284.

(6) Zanni, M. T.; Ge, N. H.; Kim, Y. S.; Hochstrasser, R. M. Two-Dimensional Ir Spectroscopy Can Be Designed to Eliminate the Diagonal Peaks and Expose Only the Crosspeaks Needed for Structure Determination. *Proc. Natl. Acad. Sci. U.S.A.* **2001,** *98*, 11265-11270.

(7) Abramavicius, D.; Voronine, D. V.; Mukamel, S. Unravelling Coherent Dynamics and Energy Dissipation in Photosynthetic Complexes by 2d Spectroscopy. *Biophys. J.* **2008,** *94*, 3613-3619.

(8) Tiwari, V.; Peters, W. K.; Jonas, D. M. Electronic Resonance with Anticorrelated Pigment Vibrations Drives Photosynthetic Energy Transfer Outside the Adiabatic Framework. *Proc. Natl. Acad. Sci. U.S.A.* **2013,** *110*, 1203-1208.

(9) Vulto, S. I. E.; de Baat, M. A.; Louwe, R. J. W.; Permentier, H. P.; Neef, T.; Miller, M.; van Amerongen, H.; Aartsma, T. J. Exciton Simulations of Optical Spectra of the Fmo Complex from the Green Sulfur Bacterium Chlorobium Tepidum at 6 K. *J. Phys. Chem. B* **1998,** *102*, 9577-9582.

(10) Dioumaev, A. K. Evaluation of Intrinsic Chemical Kinetics and Transient Product Spectra from Time-Resolved Spectroscopic Data. *Biophys. Chem.* **1997,** *67*, 1-25.

(11) Kennedy, J.; Eberhart, R. Particle Swarm Optimization. *Proc. IEEE Int. Conf. Neur. Net.* **1995**, 1942-1948.

(12) Golub, G.; Pereyra, V. Separable Nonlinear Least Squares: The Variable Projection Method and Its Applications. *Inverse Probl.* **2003,** *19*, R1-R26.